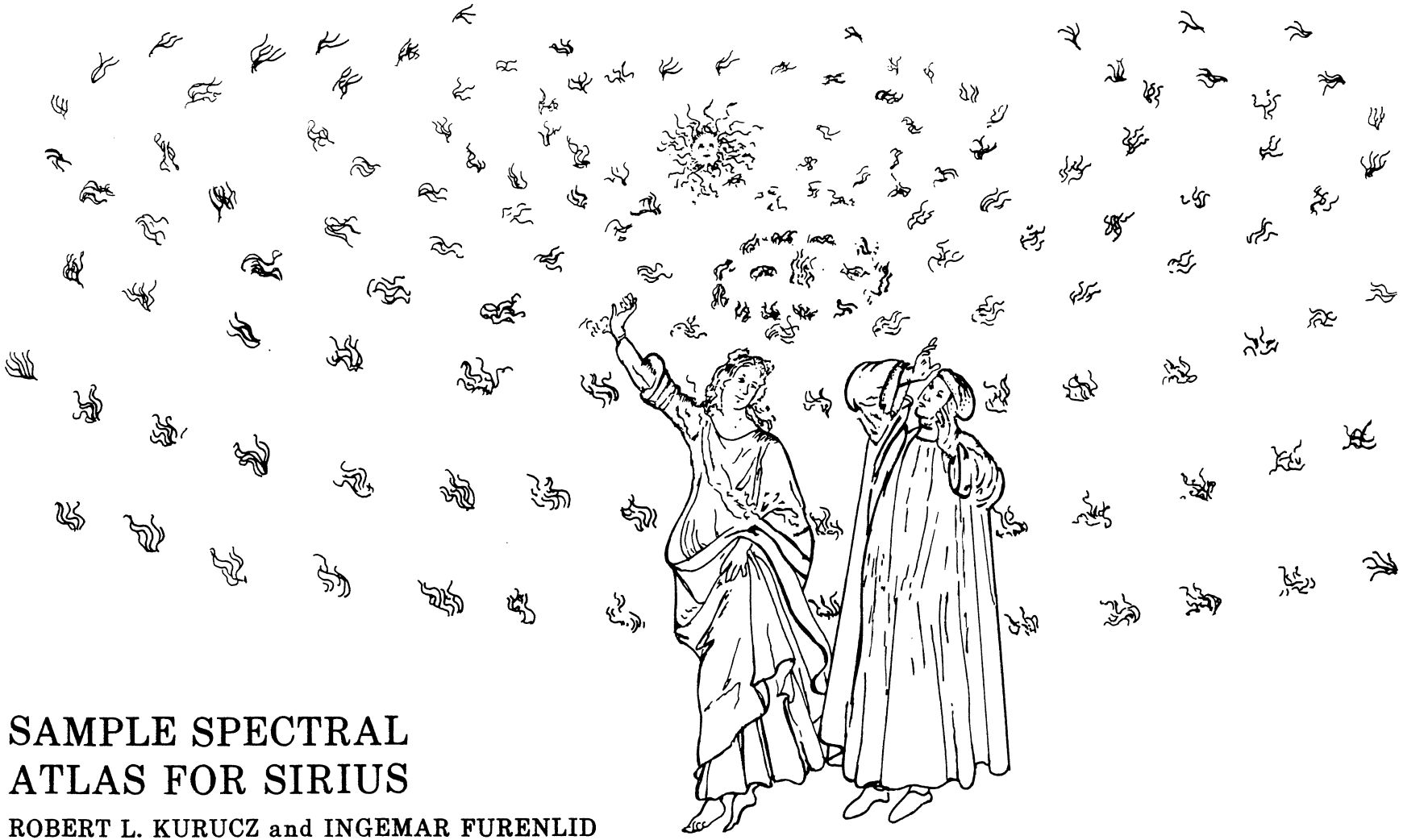

SAMPLE SPECTRAL ATLAS FOR SIRIUS

ROBERT L. KURUCZ and INGEMAR FURENLID

Smithsonian Astrophysical Observatory
SPECIAL REPORT 387

Cover illustration by Joseph Singarella after the drawing by Botticelli for the "Sphere of the Fixed Stars" in Dante's Divine Comedy.

Research in Space Science
SAO Special Report No. 387

SAMPLE SPECTRAL ATLAS FOR SIRIUS

Robert L. Kurucz
Harvard-Smithsonian Center for Astrophysics

and

Ingemar Furenlid
Kitt Peak National Observatory

November 1979

Smithsonian Institution
Astrophysical Observatory
Cambridge, Massachusetts 02138

TABLE OF CONTENTS

ABSTRACT

We present a sample spectral atlas of Sirius for the region 354 to 440 nm in which we show a photographic spectrum that resolves the line profiles and has a small-scale signal to noise better than 300. The atlas also shows a calculated spectrum that demonstrates our capabilities in spectrum synthesis. We are able to compute a spectrum, broaden it with microturbulence and rotation, transmit it through the atmosphere, convolve it with the instrumental profile, plot it together with the observed spectrum, and label each line. This approach to analyzing stellar spectra has a number of advantages over working with lists of line identifications or equivalent widths or individual line profiles: (1) The reader gets an immediate impression of the quality of the data and of blending, and many lines that appear to be single are shown to be blends. (2) The reader can much better estimate the continuum level and the total blocking to check model atmosphere predictions and assess the reliability of an abundance determined from any given line. (3) Determinations of stellar parameters and abundances can be based on all the data, not just on a small sample. (4) The reader gets an intuitive "feel" for the data and for the properties of the star, which is missing in other approaches. (5) All the data are presented and the reader who disagrees with our treatment can reanalyze them. Our programs can be used to analyze existing and future ground-based, balloon, rocket, and satellite observations of the sun and stars.

For Sirius we plot a roughly photometric spectrum at 10 nm/panel, then at 5 nm/panel with a comparison rotationally broadened calculated spectrum, then at 0.8 nm/panel with comparison unbroadened and rotationally broadened calculated spectra and line identifications. No attempt has yet been made to fit the calculated spectra to the observed spectrum. The observed spectrum has been only roughly normalized to the calculated spectrum to make it photometric. From the sample spectrum it is clear that Sirius is strongly underabundant in Ca, contrary to earlier studies, and that its abundances are roughly consistant with other metallic line stars although not extreme. There is no region of the spectrum shown here that is not produced by overlapping lines.

1979SAOSR.387.....K

SAMPLE SPECTRAL ATLAS FOR SIRIUS

Robert L. Kurucz and Ingemar Furenlid

1. INTRODUCTION

Over the past 15 years, model atmosphere calculations have developed to the point where it is almost possible to trust the calculations in some cases. The easiest type of star to model is the normal early A or late B star in which energy transport is purely radiative. Except for the minor problem of microturbulence, the physics is well understood: The difficulties now are limited to the determination of reliable line and continuum opacities and collision rates and to the development of complex computer codes. If we consider only the higher gravity stars where the collision rates are high, the statistical equilibrium calculations can be ignored altogether and we can hope to make LTE models that are reasonable representations of actual stars. Because late A and cooler stars have partially convective atmospheres, and because we do not have a good theory of convection, models of these stars must necessarily be less reliable. If we cannot produce reasonable models for the early A stars, it is not likely that reliable models for other stars can be produced.

Ideally, our calculations should be compared to a star with known energy distribution, spectrum, effective temperature, surface gravity, and abundance for each element. In addition, the star should have zero projected rotation velocity to maximize the information in the line profiles. Unfortunately, there is no star for which all this information is well known. Even in the case of the sun, only the surface gravity and the visible spectrum are well-determined. The two early A stars about which we know the most are Vega and Sirius, but for neither of them do we know any of these parameters well. We are thus forced to test the calculations while trying to determine the parameters of the star from the calculations. If the observed spectrum and energy distribution are well known, and if the calculated spectrum can reproduce the observed, this procedure is justified because any simple model that can satisfy the myriad data of a complex stellar spectrum is most likely correct.

This research was supported in part by the National Aeronautics and Space Administration grants NSG 5182 and NSG 7054. Kitt Peak National Observatory is operated by the Association of Universities for Research in Astronomy, Inc., under contract with the National Science Foundation.

Kurucz (1979a, b) has produced several grids of LTE model atmospheres that include the opacity of almost one million atomic lines in the form of statistical distribution functions. These models can be compared to observed low-resolution colors, intermediate-resolution spectrophotometry, and high-resolution spectra. The low-resolution comparisons in UBV by Buser and Kurucz (1978) and in uvby by Relyea and Kurucz (1978) indicate that the grid predictions are statistically accurate for normal early-type stars. Kurucz (1979a) has also shown that a model for Vega (T_{eff} = 9400 K, log g = 3.95, solar abundances) can be found that matches the Hayes and Latham (1975) and Tüg, White, and Lockwood (1977) spectrophotometry and that also matches the Balmer line profiles of Peterson (1968). The model does not match either the OAO 2 (Code and Meade, 1976) or TD1 (Jamar et al., 1976) observations in the ultraviolet. We show in the next paper in this series that for many lines the model also gives a reasonable match to the Copernicus far ultraviolet spectrum of Vega but there are a large number of missing lines. Of course, because of large errors in the observations, the fact of agreement or disagreement does not provide a rigorous test; and in the case of disagreement in the lower resolution observations, it is impossible to pinpoint the source of any discrepancy, which might be readily apparent at higher resolution.

It is not surprising that the model calculations should work for the most part for Vega because Vega is the archetypal normal star. It evolved in isolation. Presumably its atmosphere has the abundances of the interstellar material from which it formed. It has a relatively low projected rotation velocity and, it is hoped, a true velocity small enough not to affect the atmospheric structure. Its analysis should be straightforward.

Sirius, on the other hand, is a metallic line star that has had a complex evolution. Presumably its white dwarf companion was once the primary, then evolved, and transferred a small amount of mass to the secondary, which we now see as Sirius A.

Because the convection zones are so shallow (they also carry negligible flux), the material added to the surface has remained in the upper layers. In addition there may be element separation by diffusion as discussed by Michaud (1977, and references therein; and also Vauclair, 1976). This should cause some elements such as He, Ca, and Sc to settle below the convection zone, reducing the abundances at the surface, and should cause other elements to rise, enhancing the abundances. However, abundance analyses to date (Kohl, 1964a; Gehlich, 1969) have found He enhancements. These determinations may not be reliable because they are based on high excitation lines that are extremely model sensitive. Abundance analyses have also been performed by Strom, Gingerich, and Strom (1966) and Latham (1969). In any case no study of the atmosphere of Sirius will tell us anything significant about the abundances in the material from which it formed. Sirius does provide a good test of the diffusion theory, and, because of its nonsolar abundances, it provides an independent test of the model atmosphere calculations. If we can calculate a model for Sirius, then we can have confidence in our calculations for Pop II and intermediate population stars and for stars in galactic clusters that may have somewhat enhanced abundances. And, so long as convection is not important, we can be confident in our calculations for metallic line stars in general. Models for peculiar stars would not necessarily be reliable because of the complicated physics of magnetic fields and spots.

To test the model atmosphere calculations, we have concentrated on Vega and Sirius because they are bright, so that it is possible to get high-quality observations, because they are slow rotators, and, as described above, because we would expect, eventually, to be able to compute realistic models and spectra. We already have a reasonable model for Vega that is consistent with the spectrophotometry in the visible and infrared and with the Balmer line profiles. For the moment we are using a working model for Sirius with T_{eff} = 10,000 K, log g = 4.3, and [M/H] = 0.5, which are, approximately, the parameters $T_{eff} = 9980 \pm 200$ K and log $g = 4.31 \pm 0.04$ found by Code et al. (1976; Code, 1975) from the angular diameter, parallax, observed total flux at the earth, and the binary mass. The three times solar model should give a reasonable starting model because it overestimates the opacity of lighter elements and underestimates opacity of heavier elements. Hayes (1979) has determined a "best" energy distribution for Sirius derived from Davis (1974), Davis and Webb (1974), Hayes (1967), Hayes and Latham (1972), Johnson and Mitchell (1975), and Schild, Peterson, and Oke (1971), which is plotted in Figure 1 together with the model prediction. We see that it is inconsistent with the observations by several hundredths of a magnitude. We also show a comparison of the calculated Balmer line profiles with Peterson's measurements, which are in agreement. Our current estimate is that a model computed with the abundances appropriate for Sirius with T_{eff} = 9700 K and log g = 4.3 would give much better agreement with the spectrophotometry, especially in the infrared. As we have not yet computed such a model, the calculations presented here were made with the somewhat incorrect model.

For the spectral comparisons we are attempting to obtain complete spectral coverage of both stars to allow for relative comparisons, i.e., metallic line versus normal spectrum, as well as absolute interpretation. In the far ultraviolet, where there are many resonance lines of light elements, and where the radiation field is exponentially sensitive to temperature and thus very sensitive to the model, we have obtained Copernicus spectra. An atlas of our Copernicus spectra for Vega and Sirius will be the second paper in this series.

In the visible we are undertaking to produce high-quality photographic spectra that resolve the line profiles and have signal to noise greater than 300. High signal to noise is especially important because of rotation; weak lines that produce significant opacity and are quite important to the structure of the model are nearly washed out. The present atlas is based on a sample exposure for Sirius. We also hope to complete our spectral coverage with data from other sources.

Given the observed spectrum, we will then iterate on computing a theoretical fit to the observed spectrum, trying at the same time to correct errors and to make improvements in our line data and to determine the atmospheric parameters including all the abundances. In the example presented here we have simply adopted abundances roughly appropriate for an Am star and computed the spectrum. We have not yet iterated on any parameters or forced a match. Because the techniques we have developed should be widely useful for groundbased and satellite studies of the sun and stars, we believe it worthwhile to publish work in progress rather than waiting for the final results.

In Section 2 we described the observed spectrum. Next we discuss the spectrum synthesis computer programs in detail (Section 3). Finally, we present the sample atlas and discuss what conclusions can be drawn.

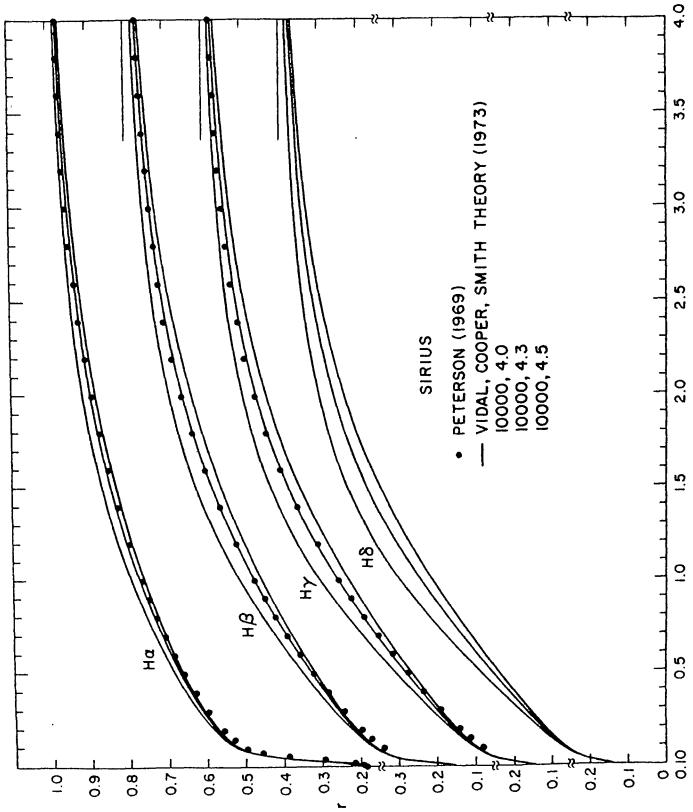

Figure 2. Comparison of the Balmer line profiles for the 10000, 4.3, 3X model compared to the observations of Peterson (1969).

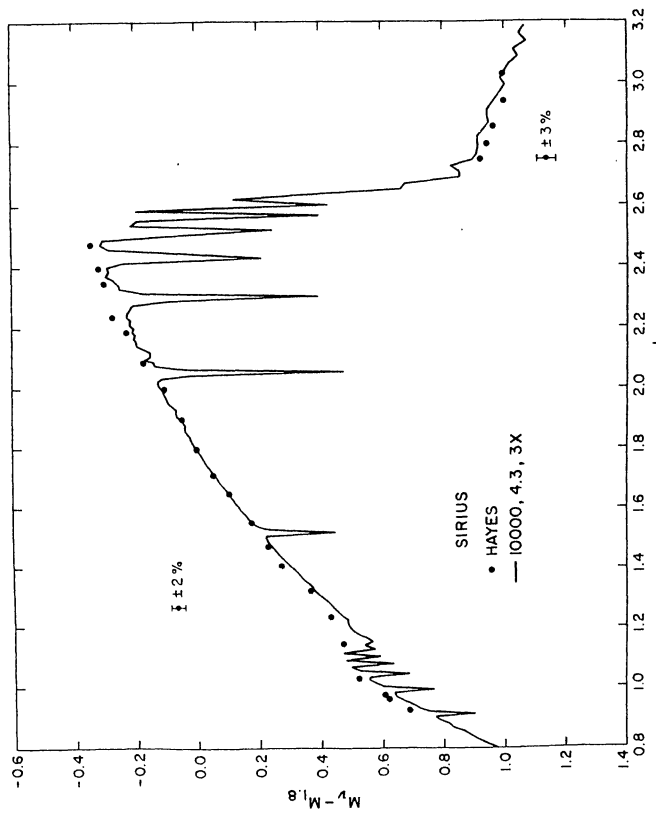

Figure 1. Comparison of the colors of the 10000, 4.3, 3X model with Hayes (1979) "best" compilation of measurements. Error bars for the observations are indicated.

1979SAOSR.387.....K

2. OBSERVED SPECTRUM

The observed spectrum of Sirius was obtained photographically by Furenlid at Kitt Peak with the 2.1-m coudé spectrograph using the feed telescope. The spectrograph camera (camera 6) and grating (grating D) combination was chosen to give maximum resolution; the average reciprocal dispersion is 1.1 Å-mm in our spectra. The slit projected on the plate has a typical width of 40 μm, corresponding to about 45 mÅ, which is adequate to resolve even weak lines in Sirius' spectrum; the smallest line half widths are approximately 200 mÅ because of stellar rotation.

IIa-0 plates were used in all cases except for plates 4986, which are of type IIIa-J. Patterns for wavelength dependent calibration were exposed onto the plates simultaneously with the stellar spectra (Furenlid, 1973). Each exposure covers 710 mm and extends over three plates stacked end-to-end in the plate holder. To avoid loss of spectral coverage at the plate ends, overlapping exposures were made; for further details of the plates, see Table 1. The spectra were traced in the PDS microphotometer at Kitt Peak and the resulting density values converted to an arbitrary intensity scale.

Table 1. Exposures.

Plate no.	UT date	Emulsion type	Exp. time (min)	Projected slit Width (μm)	Projected slit Height (μm)	Wavelength region (nm)
4994 A	14 Nov. 1974	IIa-0	25	40	1220	353 - 375
7585 A	17 Feb. 1978	IIa-0	40	40	5070	370 - 392
4994 B	14 Nov. 1974	IIa-0	25	40	1220	380 - 395
7585 B	17 Feb. 1978	IIa-0	40	40	5070	392 - 415
4986 B	12 Nov. 1974	IIIa-J	14	35	1220	410 - 422
7585 C	17 Feb. 1978	IIa-0	40	40	5070	415 - 441

From the data in Table 1 on slit width and slit height projected on the plate, we can estimate the output signal-to-noise (S/N) in the spectra (Furenlid, 1978). An untreated IIa-0 plate has a peak S/N of around 23 per 1000 μm^2, where S/N scales as the square-root of the area of measurement (Latham, 1974). For IIIa-J plates, the corresponding S/N is around 50. The projected slit area of one resolution element on plates 7585 amounts to around 200,000 μm^2, resulting in a S/N of 325. The plates from exposures 4986 and 4994 have projected slit areas of around 49000 μm^2, which gives a S/N of 350 and 160, respectively. After smoothing by Fourier filtering and some allowance for the exposures not being optimal, we have S/N in the data of approximately 550, 600, and 250 for plates 7585, 4986, and 4994, respectively. These values of S/N refer to small-scale fluctuations (grain noise). Fluctuations on a large scale, i.e., one or several centimeters, are also present but are of less importance in line photometry. The detection limit for the weakest lines should be in the neighborhood of 1 mÅ. Scattered light, which has not been allowed for and which we estimate to be 2%, introduces a systematic error that increases with line depth.

A sample of the spectrum showing the Ca K line before and after smoothing is shown in Figure 3. In the Fourier smoothing the length of each microphotometer scan was expanded to the next higher power of 2 by linearly interpolating from the last point to the repeated first point at 2^n+1. The spectrum was Fourier transformed and a log power spectrum was plotted as shown in Figure 4. The noise level and a cutoff function were subjectively determined. In the plot the heavy horizontal line is the adopted noise level and the heavy sloped line is the adopted cutoff function. It is apparent from the plot that the noise level is at least a factor of 300 below the power level of the central lobe and that a first sidelobe is clearly visible. To get an impression of what we should expect to see, we computed a power spectrum from our calculated spectrum rotationally broadened to V sin i = 16 km/sec as shown in Figure 5. A noiseless completely resolved observed spectrum should produce a similar power spectrum. Gray (1973) and Smith (1976) have discussed sidelobes in power spectra of individual lines. It is apparent that signal to noise of 300 to 1000 is required to show the first sidelobe in actual observations, and signal to noise of 10000 to show the second and third. The power spectrum was multiplied by the smoothing function

$$P_{smooth} = P_{raw} \frac{CUTOFF}{CUTOFF + NOISE}$$

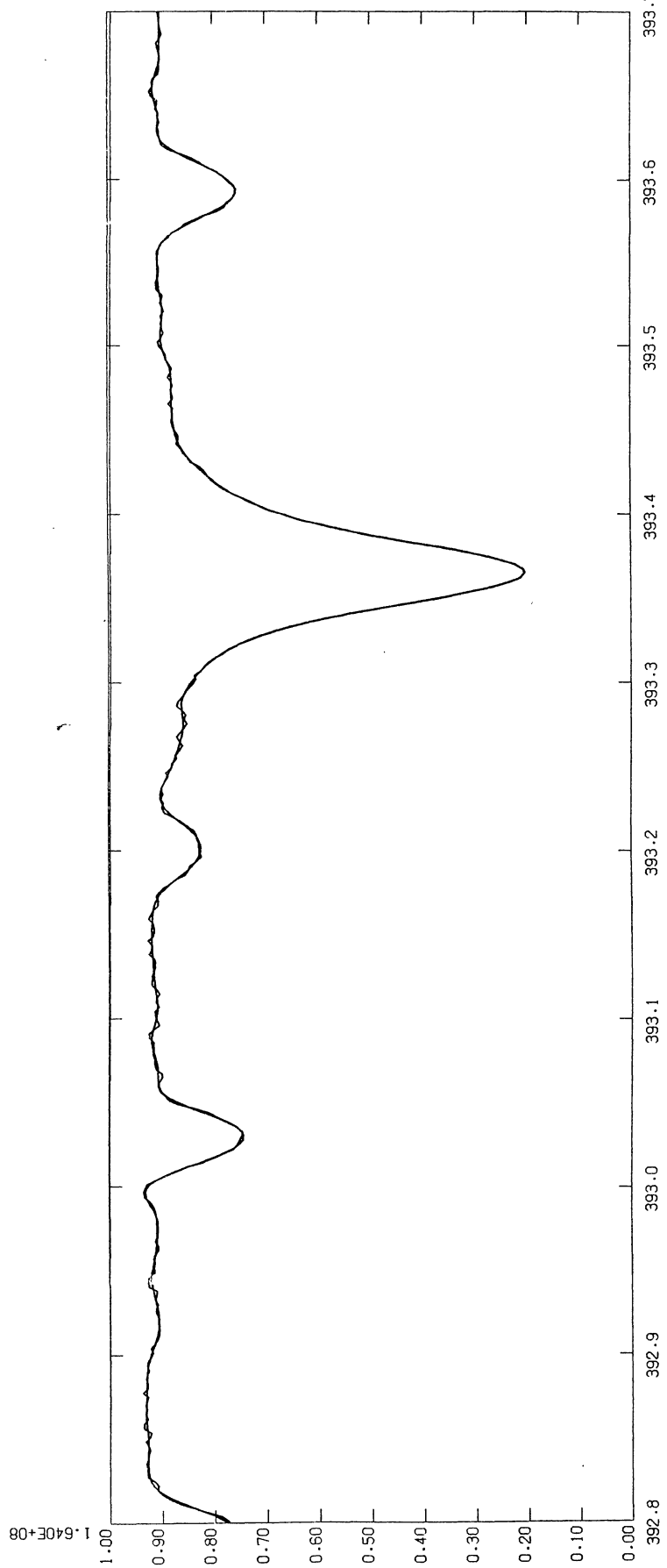

Figure 3. A sample section of the observed spectrum showing the Ca II K line before and after smoothing.

1979SAOSR.387.....K

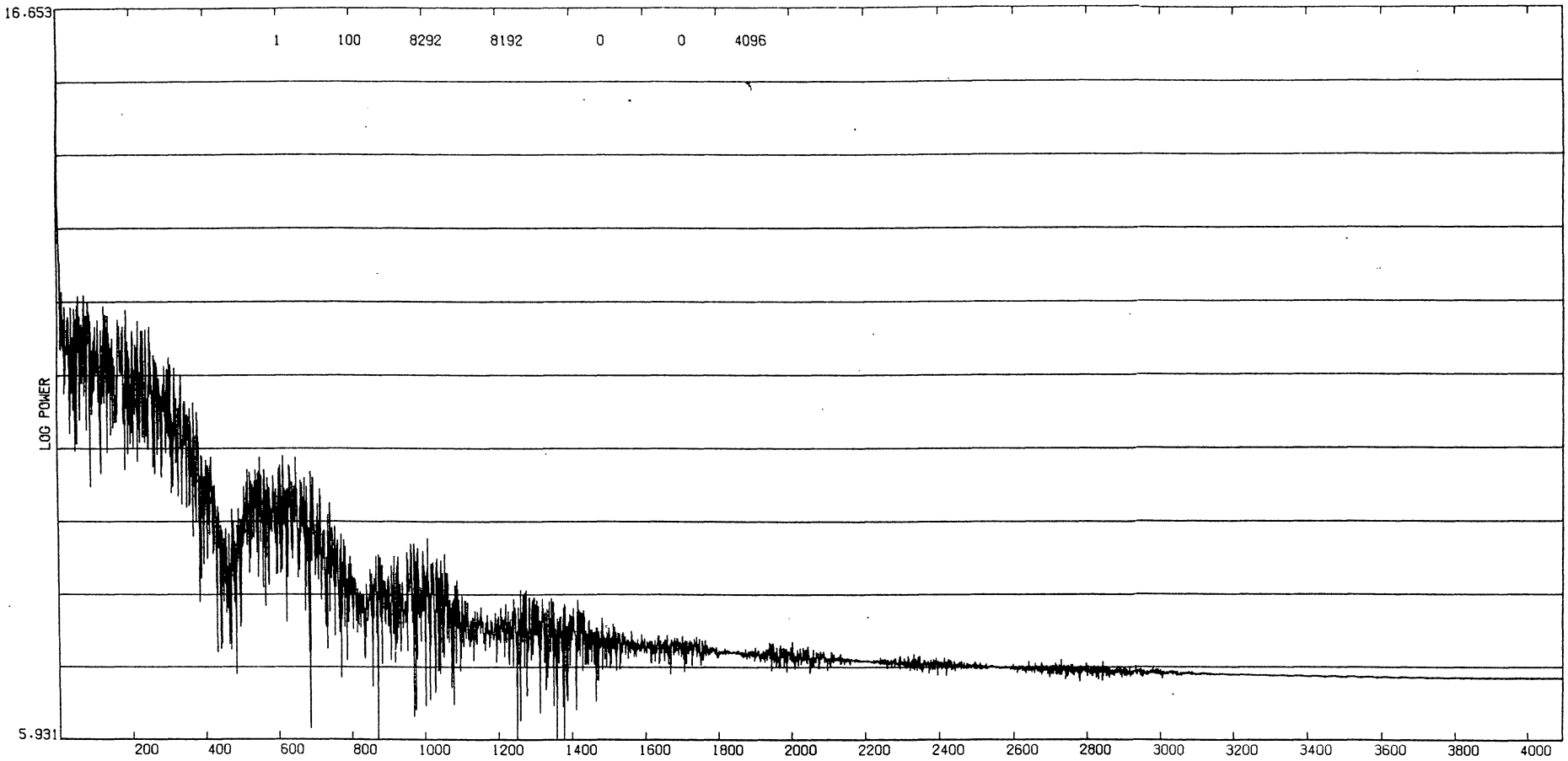

Figure 4. An example of rotational side lobes in the log power spectrum of 8192 points of the calculated spectrum from 420.2 to 436.6 nm with a spacing of 2 pm. (Every other calculated point.) The calculated spectrum has been rotationally broadened for V sin i = 16 km/sec. Signal to noise of 300 to 1000 is required to show the first side lobe in actual observations, and signal to noise to 10000 to show the second and third.

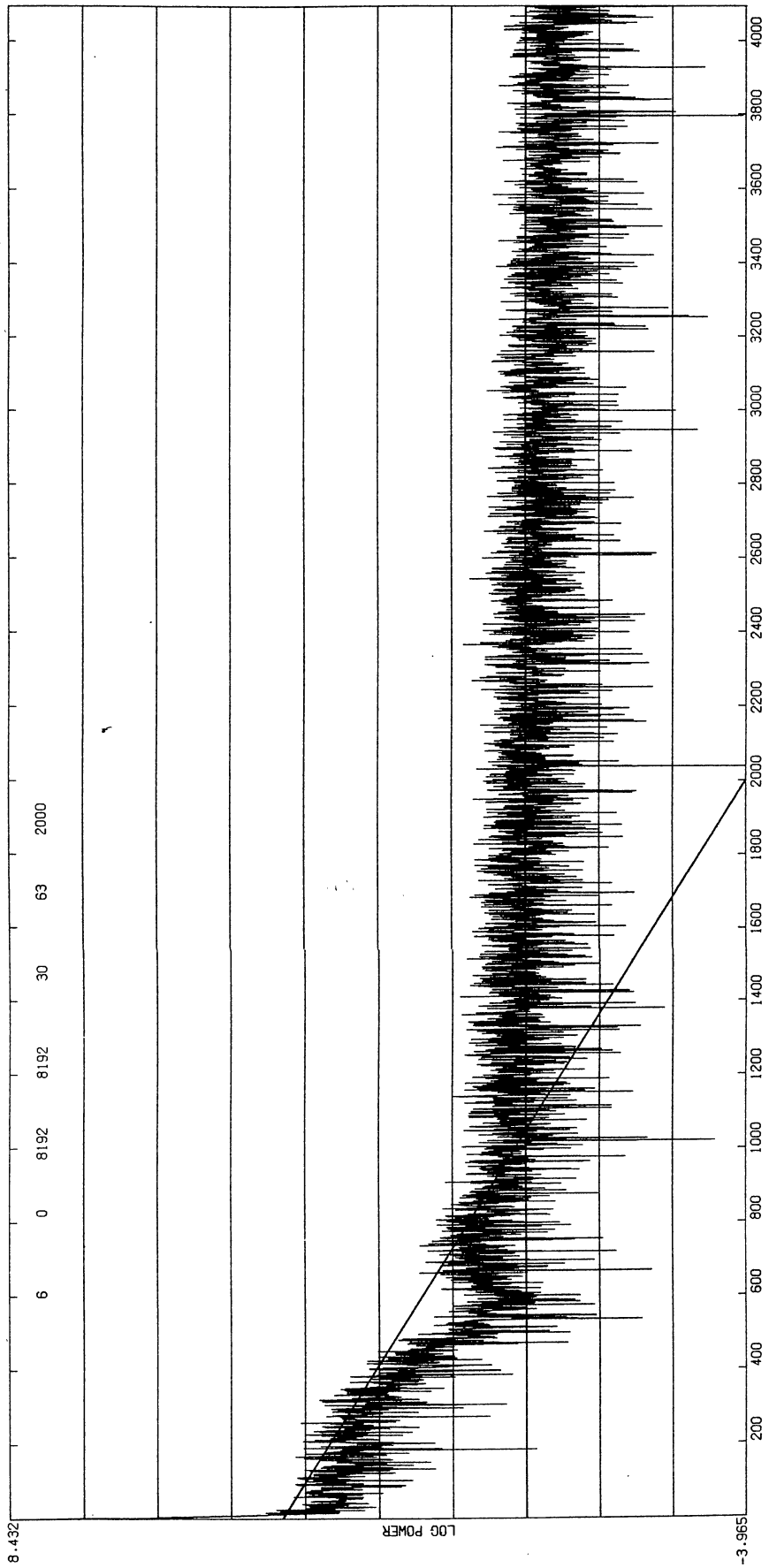

Figure 5. The power spectrum of 8192 points of the observed spectrum for 418.5 to 439.1 nm. The sample interval is 25% larger than in Figure 2 so the frequencies of the minima are 25% larger. Note that a first sidelobe is clearly visible and that higher sidelobes are obscured by noise. The heavy horizontal line is the adopted noise level and the heavy sloped line is the adopted cutoff function for smoothing

$$P_{smooth} = P_{raw} \frac{CUTOFF}{CUTOFF + NOISE} .$$

to eliminate the noise (and also some information between the first and second sidelobes). The power spectrum was then transformed back to the smoothed spectrum.

The wavelength scale was originally set by assigning a number of wavelengths from Kohl's (1964b) line list to observed minima and then fitting a third-order polynomial. We have subsequently made several improvements using the calculated spectrum. As this project procedes we expect to be able to use all the features that can be well computed to give a definitive wavelength fit. At the present time there are errors as large as 0.003 nm. The power of the spectrum synthesis procedure is readily apparent here. Several of the features that were used in the first fit because they were thought to be well-defined lines turned out to be complicated blends that rotational broadening had merged into single features.

The six scans were combined into one continuous scan by use of small sections of the poorer quality scans to interpolate between the better plates and by adjusting the intensities of each plate to force a match at the boundaries. Then, scaling factors were linearly interpolated roughly every 2.5 nm to force the spectrum to an approximate match with the calculated spectrum. Because of the rapid change in the sensitivity of the plates in the ultraviolet and in the transmission of the atmosphere and because of the linear interpolation, the wavelength variation of the intensity scale is not reliable enough for determining Balmer profiles. When our calculations have been fitted to the observed spectrum and when we have compared the photoelectric measurements, we may be able to determine the hydrogen line profiles. Also, as mentioned above, no correction has yet been made for scattered light, which is on the order of 2%.

1979SAOSR.387.....K

3. SPECTRUM SYNTHESIS PROGRAMS

The spectrum synthesis computer programs have been under development since 1965. The algorithms for computing the total line opacity are extremely fast because maximum use is made of temperature and wavelength factorization and pretabulation. Below we present a detailed description of these programs.

First, quantities that need be computed only once for each model atmosphere are pretabulated. A model is read in; departure coefficients are included if the model is non-LTE. The continuum opacity is tabulated at wavelength points on both sides of every photoionization edge and throughout the Balmer and Paschen continua for later use in estimating the strength of line wings relative to the continuum. The atomic and molecular number densities divided by partition functions are pretabulated for later use in Boltzmann equations. Doppler velocities are also pretabulated for each atom and molecule with allowance for depth-dependent microturbulence.

Line data are divided into two groups for treatment. In the first group, the lines must have a source function that is the Planck function B_ν or another fixed function that is the same for all the lines and that approximately accounts for non-LTE at the surface. In the second group each line has its individual source function, which is taken to be B_ν if the calculation is LTE.

The first group of lines is used in the second computational stage to produce a summed line absorption coefficient for the wavelength interval of interest, which may be specified for either air or vacuum wavelengths. Because the central wavelength of the interval is used to pretabulate a number of quantities such as doppler width, the width of the interval cannot be so large that the use of λ_{center} instead of λ causes a significant error. Typically, 20-nm intervals are used in the visible and 10-nm intervals in the ultraviolet.

The Kurucz and Peytremann (1975) line list provides the basic data and is combined with a list of additional lines, corrections, and deletions. The program extracts a smaller list of lines that fall in or overlap the wavelength interval. For each line, the air or vacuum wavelength, the exact upper and lower energy levels, and the gf value must be given. Other data may also be specified on the correction cards. These are the upper and lower J, labels for the upper and lower level, radiative, Stark, and van der Waals damping constants, fractional isotopic abundances for treating isotopic lines, and additional comment and reference fields. Departure coefficient indices for the upper and lower levels, line strength, partial redistribution, and autoionization parameters may also be specified for later use in the individual line calculations. Lines may also be specified as coronal for later treatment in the coronal approximation. Pseudolines may be read in for photoionization edges that serve to move the edge to the point at each depth where the line series merges into a continuum.

If the damping constants for a line are not read in, the following approximations are used as defaults:

Radiative:

$$\Gamma_R = 2.223\text{E}13/\lambda^2_{center} \qquad \text{for } \lambda_{center} \text{ in nm;}$$

Stark:

$$\Gamma_s = 1.0\text{E}{-8}\, n^5_{eff}\, N_e \ ,$$

which is a fit by Peytremann (1972) to detailed calculations by Sahal-Brechot and Segre (1971). Here, n_{eff} is the effective quantum number of the upper state,

$$n^2_{eff} = \frac{R\, Z^2_{eff}}{E_{ion} - E_{upper}} \ ,$$

where R is the Rydberg energy, Z_{eff} is the effective charge (= 1 for Fe I, 2 for Fe II, etc.), and E_{ion} is the ionization potential. If the upper level is above the ionization potential because it ionizes to an excited level of the parent, n_{eff} is set to 5.

van der Waals: Starting with the treatment in Aller (1963) and taking into account the polarization of H, He, and H_2 we adopt

$$\Gamma_W = 17\left[\frac{8\,kT(1/A+1/1)}{\pi M}\right]^{0.3}\left[6.63E\text{-}25\,\frac{e^2}{h}\left(\langle r^2\rangle_{up} - \langle r^2\rangle_{lo}\right)\right]^{0.4} N_H$$

$$+ 17\left[\frac{8\,kT(1/A+1/4)}{\pi M}\right]^{0.3}\left[2.07E\text{-}25\,\frac{e^2}{h}\left(\langle r^2\rangle_{up} - \langle r^2\rangle_{lo}\right)\right]^{0.4} N_{He}$$

$$+ 17\left[\frac{8\,kT(1/A+1/2)}{\pi M}\right]^{0.3}\left[8.04E\text{-}25\,\frac{e^2}{h}\left(\langle r^2\rangle_{up} - \langle r^2\rangle_{lo}\right)\right]^{0.4} N_{H_2} \quad .$$

Then, assuming that the atomic weight A is much greater than 4 and that the mean-square-radius of the lower level $\langle r^2\rangle_{lo}$ is small compared to $\langle r^2\rangle_{up}$, and by standardizing to T = 10,000 K, we find

$$\Gamma_W = 4.5E\text{-}9\,\langle r^2\rangle^{0.4}\left[N_H + 0.42\,N_{He} + 0.85\,N_{H_2}\right]\left(\frac{T}{10000}\right)^{0.3} \quad .$$

These approximations assume a single optical electron and that the f sum rule yields 1, which is not in fact the case for the d^n levels of the iron group. If the van der Waals constant is read in, it is expressed as Γ_W/N_H at 10,000 K for broadening by H only,

$$\Gamma_W/N_H = 4.5E\text{-}9\,\langle r^2\rangle^{0.4} \quad ,$$

and the He and H_2 dependencies are computed. We have fit the default for iron group elements, assuming that strong lines have a 4p upper level, to our calculated wavefunctions for 4p,

$$\langle r^2\rangle = (45\text{-}S)/Z_{eff} \quad ,$$

where S is the atomic number of the sequence, i.e., 26 for the iron sequence. For other atoms the hydrogenic form is used:

$$\langle r^2\rangle = 2.5\left(\frac{n^2_{eff}}{Z_{eff}}\right)^2 \quad .$$

If the upper level is above the ionization potential $\langle r^2\rangle \equiv 25$. For molecules we have arbitrarily adopted the defaults

$$\Gamma_S/N_e \equiv 1.0E\text{-}5 \quad \text{and} \quad \Gamma_W/N_H \equiv 1.0E\text{-}7/Z_{eff} \quad .$$

The program makes a new smaller list of lines that fall within the wavelength interval or overlap the ends. For each depth in the model, it reads the pretabulated number densities divided by partition functions, N/U, and the doppler velocities, which are converted to doppler widths by using the central wavelength or frequency. A buffer is set up that represents the whole wavelength interval plus 1000 points at each end for overlapping lines. A 20-nm interval in the visible with a point spacing of 1 pm thus has a 22001-point buffer. The program goes through the line list rounding the line center wavelength to the nearest point in the buffer so that each line is symmetric about the central point and only one wing need be computed. This approximation also means that the spectrum can be computed only in high resolution. The line absorption coefficient is divided into three factors,

$$\ell_\nu = \left[\frac{\pi e^2}{mc}\,\frac{N}{U}\,\frac{1}{\rho}\,gf\,\frac{1}{\sqrt{\pi}\,\Delta\nu_D}\left(1 - e^{-h\nu/kT}\right)\right]\left[e^{-E/kT}\right][H(a,v)] \quad ,$$

the second and third of which are expensive to compute and are less than or equal to 1. Stimulated emission is computed only once using the central frequency of the interval. The line absorption coefficient is initially set to the first factor. If this value is less than 0.001 times the pretabulated approximate continuum opacity, the line is discarded from the current depth. The Boltzmann factor is otherwise multiplied in and the test is repeated. If the line passes, the damping parameter

$$a = \frac{\Gamma_R + \Gamma_S + \Gamma_W}{4\pi\,\Delta\nu_D}$$

is evaluated and the Voigt function is computed at successive steps away from line center for $v = \frac{\Delta\lambda}{\Delta\lambda_D}$ until the wings fall below 0.001 of the continuum. Table lookup is used to find $H(a,v) \simeq H_0(v) + aH_1(v)$, where H_0 and H_1 are pretabulated to give an accuracy better than 2% for $a < 0.1$. An upper limit of 0.25 is placed on a, but typical values

1979SAOSR.387.....K

range from 0.01 to 0.001. The program saves the line-center absorption coefficient and all the parameters for every line used. After going through all the layers in the model atmosphere an array of, say, 20001 by 64 has been computed. This is transposed and written out one wavelength at a time for use in computing the spectrum. The line center opacity is also written out for each line for subsequent computation of the central depth of each line.

The next stage of the calculation uses a version of the model atmosphere program ATLAS (Kurucz, 1970) to compute the non-LTE line opacity and source function, add in the LTE line opacity and source function, add the continuum opacity and source functions and then compute the intensity or flux at each wavelength point. In this version of ATLAS, departure coefficients have been inserted in the partition functions, the Saha and Boltzmann equations, and the opacities. If the model atmosphere is LTE the departure coefficients are all set to unity in the calculation. To save computation, continuum quantities are pretabulated at the middle and ends of the interval, or for any subinterval formed by an opacity discontinuity, and interpolated to each wavelength parabolically. In complete redistribution the following source function is used,

$$S_\nu = \left[\kappa_\nu \bar{S}_\nu + \sigma_\nu J_\nu + \ell_\nu (1-f)\, S_\nu^L + \ell_\nu f J_\nu + \Sigma\, \ell_\nu^i S_\nu^i\right] / (\kappa_\nu + \sigma_\nu + \ell_\nu + \Sigma\, \ell_\nu^i) \quad ,$$

where κ_ν and σ_ν are the continuum absorption and scattering opacities, ℓ_ν and S_ν^L are the summed line opacity, which has already been calculated, and its source function, respectively, and ℓ_ν^i and S_ν^i are the individual line absorption coefficients and source functions produced in this stage of the calculation. The f is a depth-dependent function that allows treatment of part of the line opacity as scattering. We normally make the approximation that J_ν is computed only for the continuum and is interpolated, and also that the line opacity is pure absorption, so that the source function is

$$S_\nu = \left[(\kappa_\nu + \sigma_\nu)\, S_\nu^{cont} + \ell_\nu S_\nu^L + \Sigma\, \ell_\nu^i S_\nu^i\right] / (\kappa_\nu + \sigma_\nu + \ell_\nu + \Sigma\, \ell_\nu^i) \quad .$$

Before the point by point calculation begins, the non-LTE line list is read in wavelength order and lines that overlap the wavelength interval are selected. For each line there is a strength parameter that limits the extent of its wings to 0.1, 0.3, 1., 3., 10., 30., or 100. nm. The default if the parameter is not specified is 0.1 nm. The lines are divided into seven groups and stored in an array, starting with the strongest. As each point in the wavelength interval is computed, only those lines are considered whose wings could reach to the wavelength. Lines included in the non-LTE list at the present time are H, He, C, Mg, Al, and Si, with line series extrapolated to high n so that lines merge smoothly into continua, as well as a few other lines. Merging of a series into a continuum is treated by moving the edge redward at each depth to the point of merging, then not computing higher n lines. Hydrogen lines are computed using a new routine from Peterson (1979) that approximates the Vidal, Cooper, and Smith (1973) profiles, works to high n, and includes doppler broadening, resonance broadening, van der Waals broadening, and fine-structure splitting. Autoionization lines have Shore parameter Fano profiles. Other lines have Voigt profiles that are computed accurately for any a. The lines occur at their exact wavelengths. Departure coefficients for levels that are higher than have been computed are assumed to be the same as those for the ground state of the next higher stage of ionization. A few strong lines can be treated with approximate partial redistribution but the computer cost increases dramatically. It is also possible to use the coronal approximation and ionization tables for highly ionized lines if the model has a corona.

Either surface flux or surface intensity at up to 20 angles can be computed. In this calculation 17 angles were used from $\mu = 1.0$ to 0.01. For each point in the spectrum both the spectrum and the continuum are written out. Finally the line center residual intensity is computed for all the lines that were used in the calculation.

In the next stage, the spectrum can be rotationally broadened. At each wavelength the spectrum is interpolated to 100 μ values evenly spaced from 0.995 to 0.005. A rectangular grid is placed over the stellar disk and for the given V sin i the μ index and the doppler shift in wavelength steps are computed for each point. These pairs of numbers are sorted in $\Delta\lambda$, summed, and normalized to integrate to the flux. For V sin i = 0 this simply amounts to computing flux integration weights. A buffer is then set up that is longer than the spectrum, the intensity-interpolated spectrum is read in, one wavelength at a time, and is distributed among the neighboring wavelengths according to the broadening indices and is added to the buffer. For normal spherical stars, symmetries are used to reduce the number of calculations but the method will work for any shape star or even binaries.

In the present case we found a 100 by 100 point grid sufficient for 0 km/sec and for 16 km/sec rotational broadening, but denser grids, finer wavelength spacing in the spectrum, or finer interpolation in μ can be used to increase the accuracy.

Other forms of broadening (macroturbulent, instrumental) are treated in similar fashion. The broadening function is defined at integral values of the point spacing. Then the spectrum is read in, one wavelength at a time, redistributed among neighboring wavelengths, and added to the buffer for the new spectrum.

Other complications that can be introduced in the spectrum synthesis are interstellar or terrestrial atmospheric absorption and a depth-dependent doppler shift.

1979SAOSR.387.....K

4. DESCRIPTION AND DISCUSSION OF THE ATLAS

In this section we present the atlas in three forms, in 10-, 5-, and 0.8-nm panels, and we discuss qualitative conclusions that can be derived from this preliminary work.

In Figure 6 we plot the observed spectrum in a compressed format on nine 10-nm panels. This plot is approximately photometric with all panels on the same scale and full scale with H_λ = 2.062E8 ergs cm/sec/ster/nm at the surface of Sirius. The thin line is the calculated continuum level. Note that there is no region in the observed spectrum where the continuum is visible.

Figure 7 is plotted at twice the scale (5-nm panels) so that we can show both the observed and rotationally broadened calculated spectrum. The spectrum was computed using the model described in the introduction assuming 2 km/sec microturbulent velocity but with abundances changed to approximately those of a metallic line star as follows: elements lighter than Na, solar abundance; elements lighter than Ca, 3 times solar; Ca and Sc 1/10 solar; and elements heavier than Sc, 10 times solar. Flux spectra were computed with no broadening and with the 16 km/sec rotational broadening found by Kurucz et al. (1977). We have not included the minor instrumental broadening in this sample calculation. The vertical scale in each panel has been adjusted so that the highest point of the continuum is at the top except for the region of the Balmer confluence where a level near the Balmer continuum is used. The hydrogen lines and many of the metal lines agree remarkably well. Many of the calculated lines are too strong.

Finally, Figure 8 presents all the details of the calculation in 0.8-nm plots. Both the unrotated and rotationally broadened spectra are plotted and lines with depths greater than 1% in isolation are labelled.

An overall impression is that there is remarkable agreement, that there are generally calculated features corresponding to the features in the observed spectrum, although not necessarily the weakest features, and that the calculated features are too

Figure 6. The observed spectrum plotted in 10-nm panels. The spectrum has been roughly normalized to the spectrum computed from the model atmosphere, which, in turn, roughly matches the spectrophotometry. The horizontal line is the continuum level in the calculation. Full scale is H_λ = 2.062E8 ergs/cm^2/s/ster/nm at the surface of Sirius.

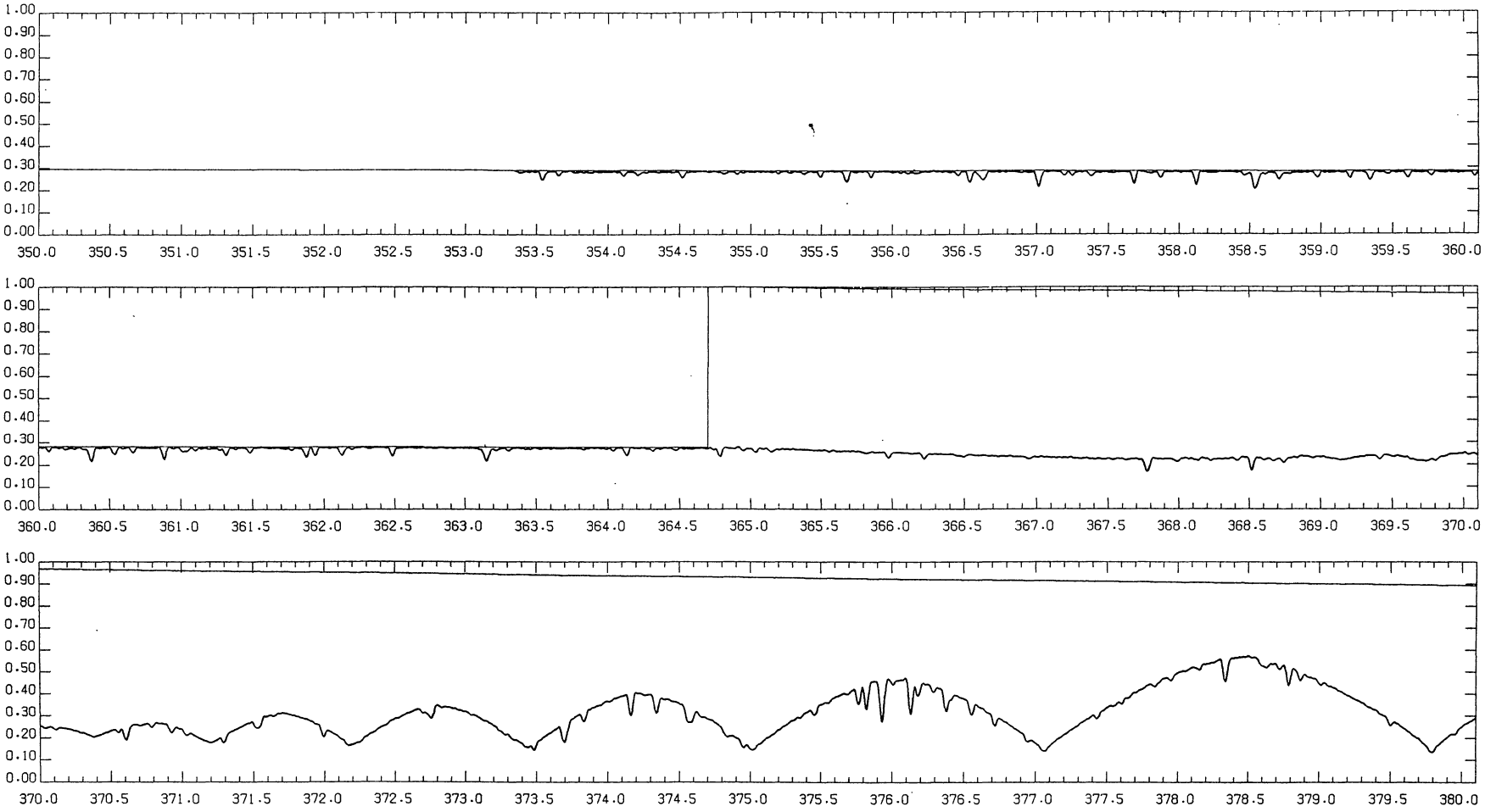

Figs. 6 (3)

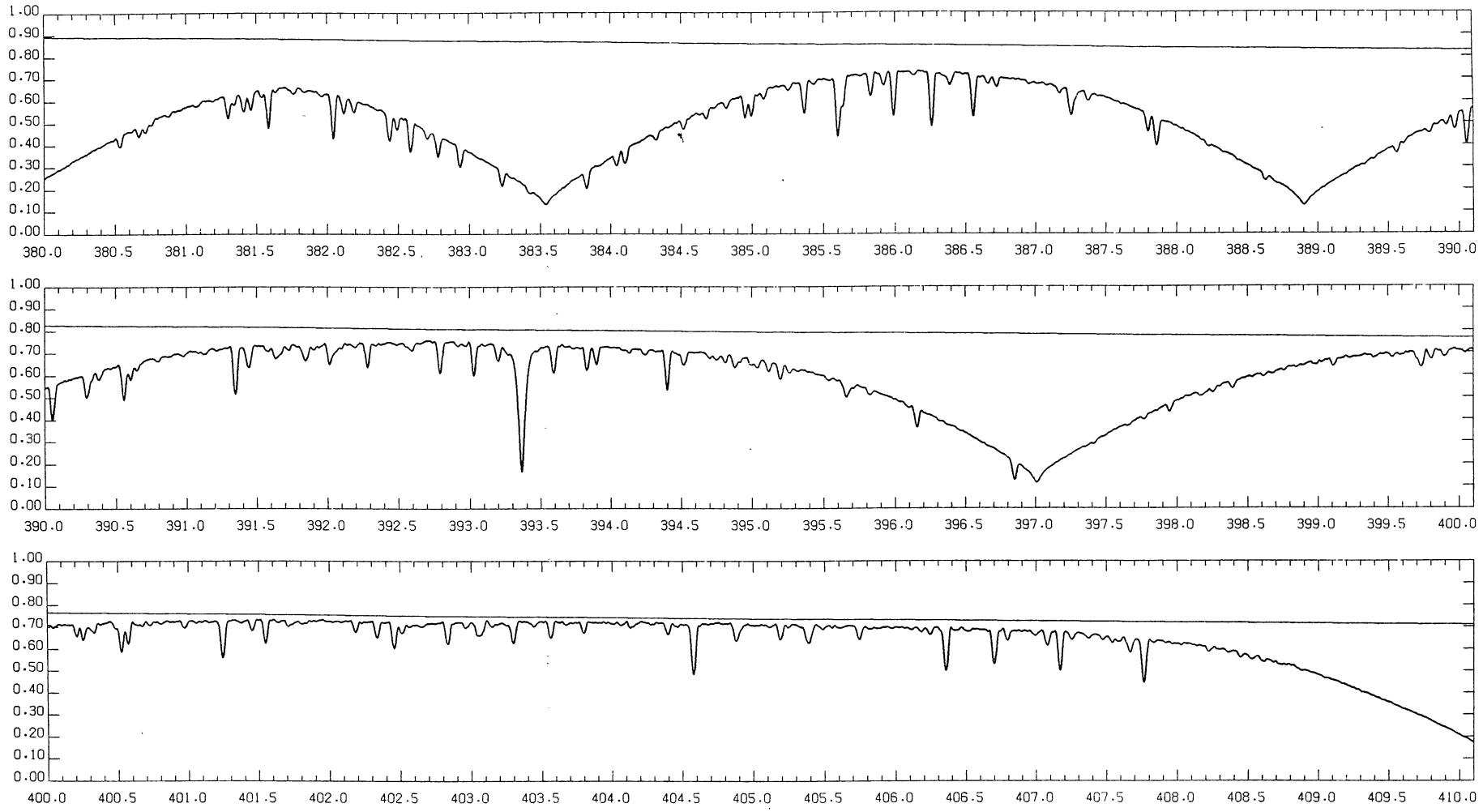

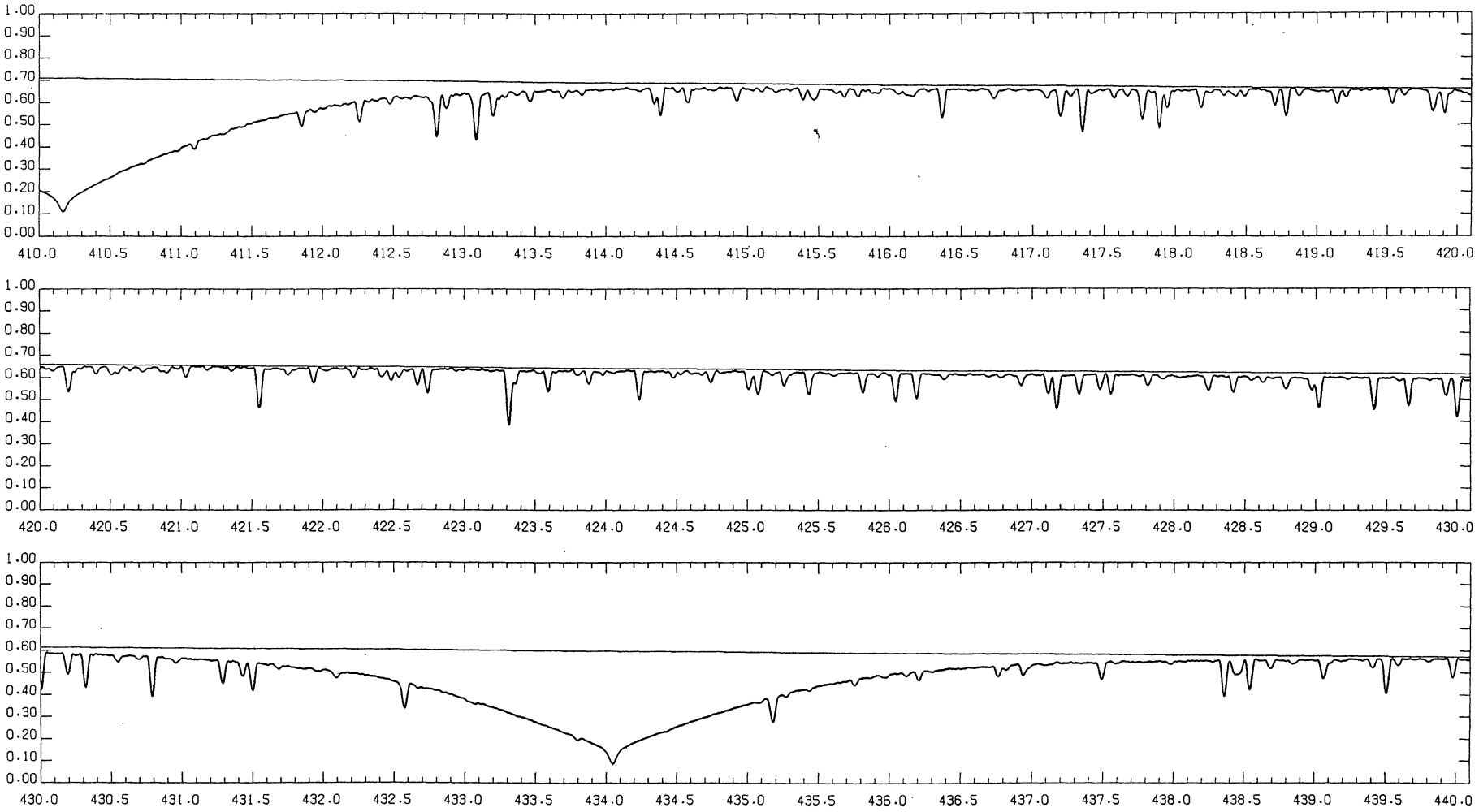

Figure 7. The calculated continuum and 16 km/sec rotationally broadened spectrum, and the observed spectrum (heavy line) plotted in 5-nm panels. No attempt has been made in the calculation to force a match to the observed spectrum but the observed spectrum has been roughly scaled to the calculated spectrum. The observed hydrogen line profiles are not reliable in this scaling.

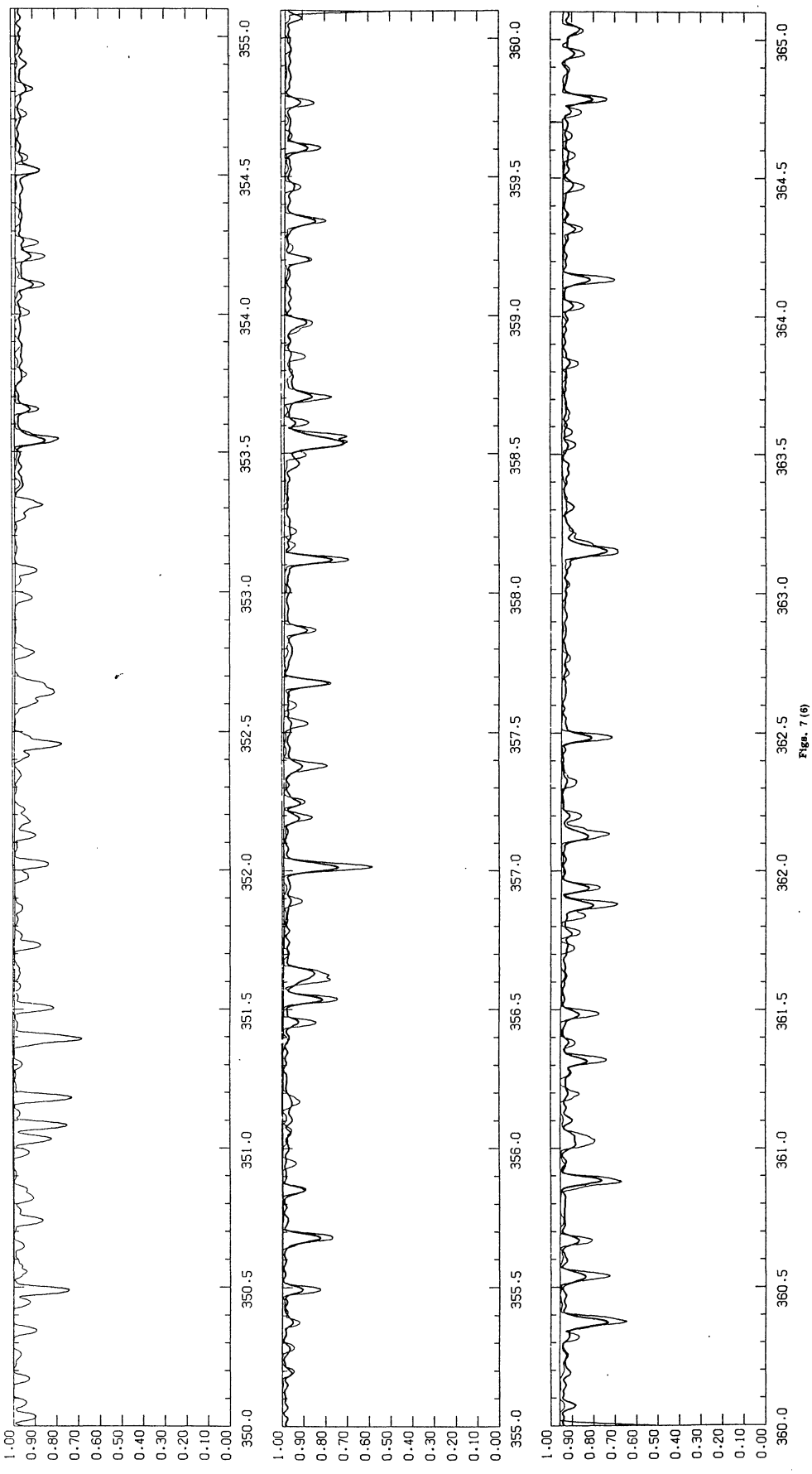

Figs. 7 (6)

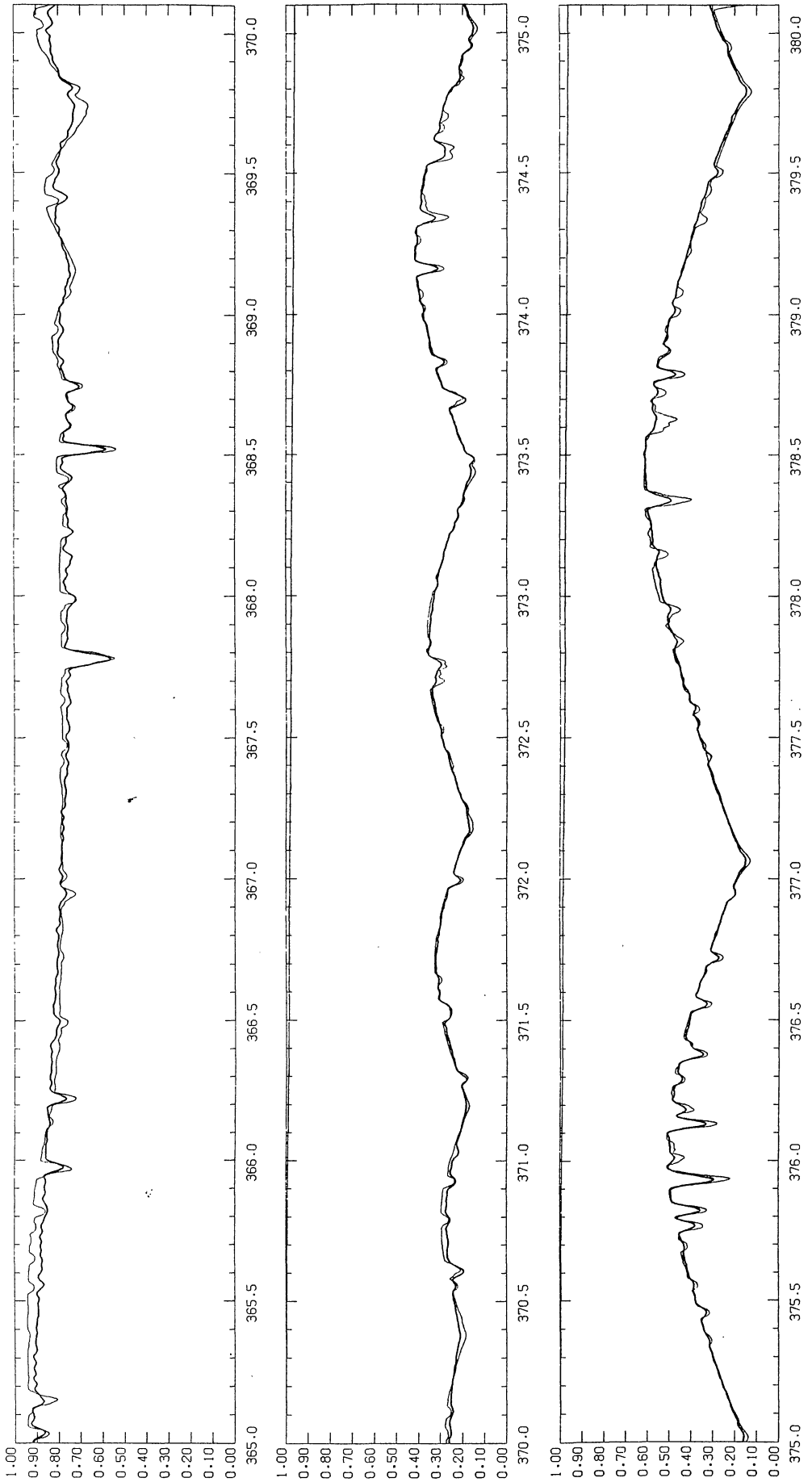

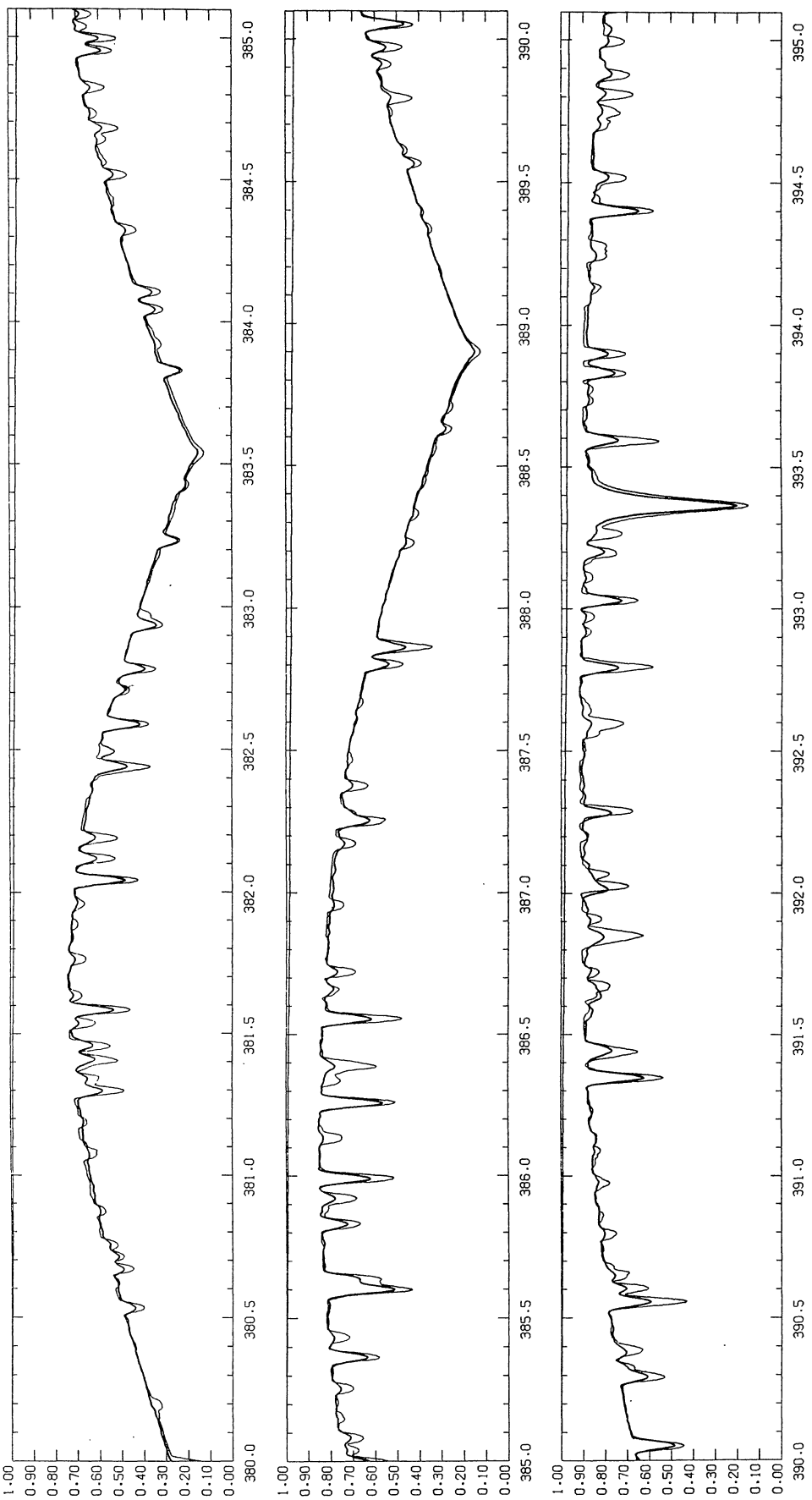

1979SAOSR.387.....K

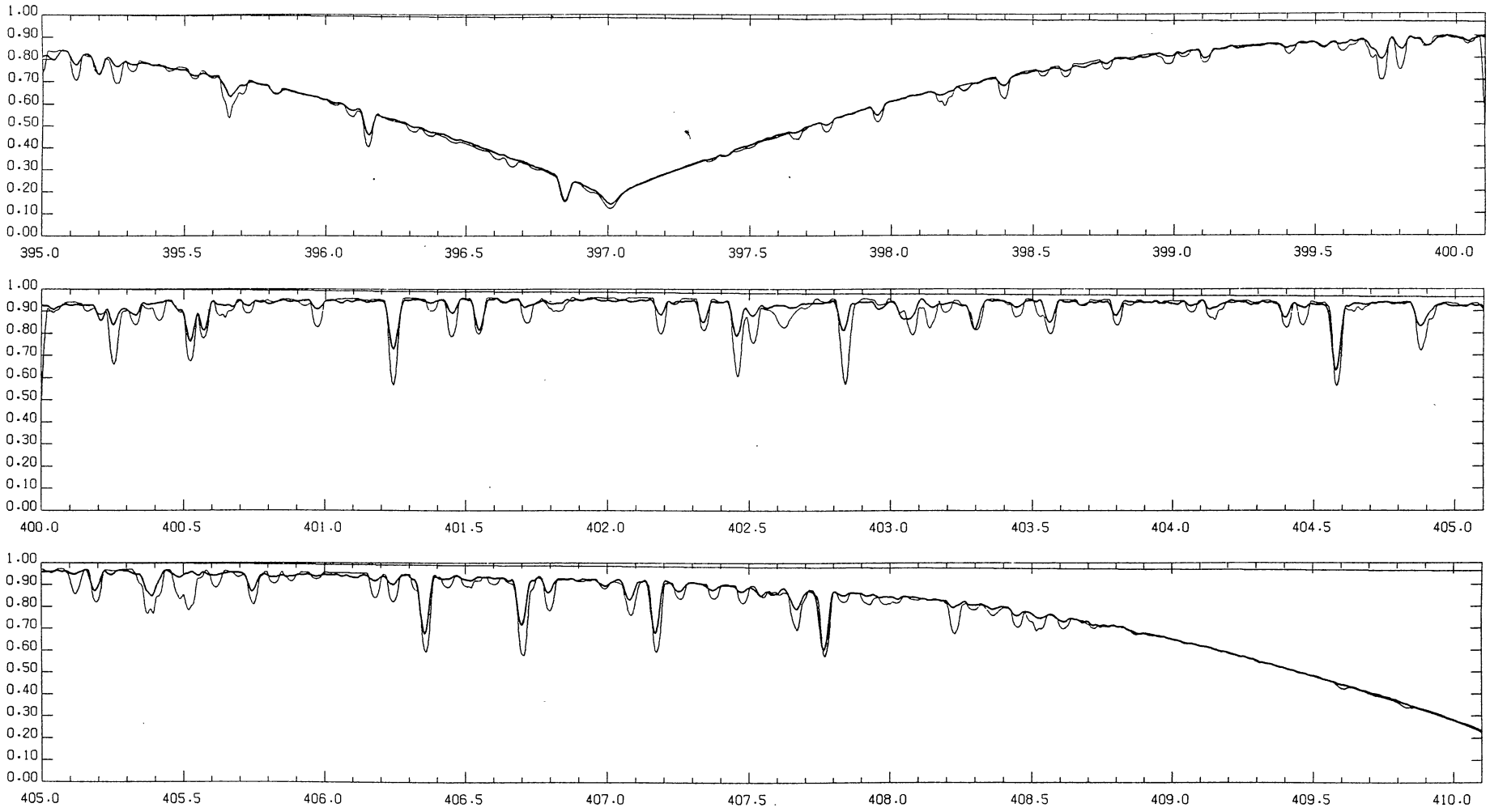

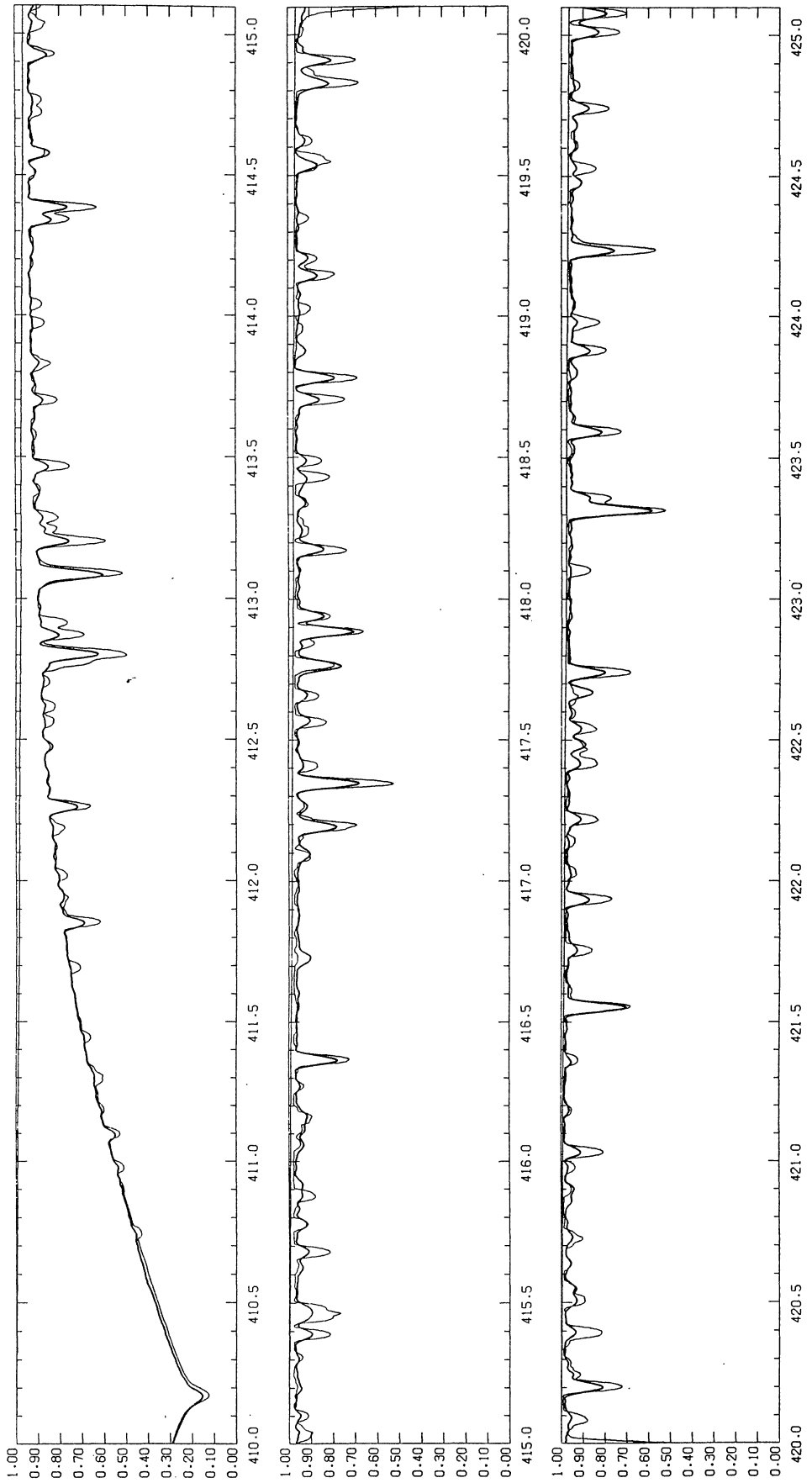

1979SAOSR.387.....K

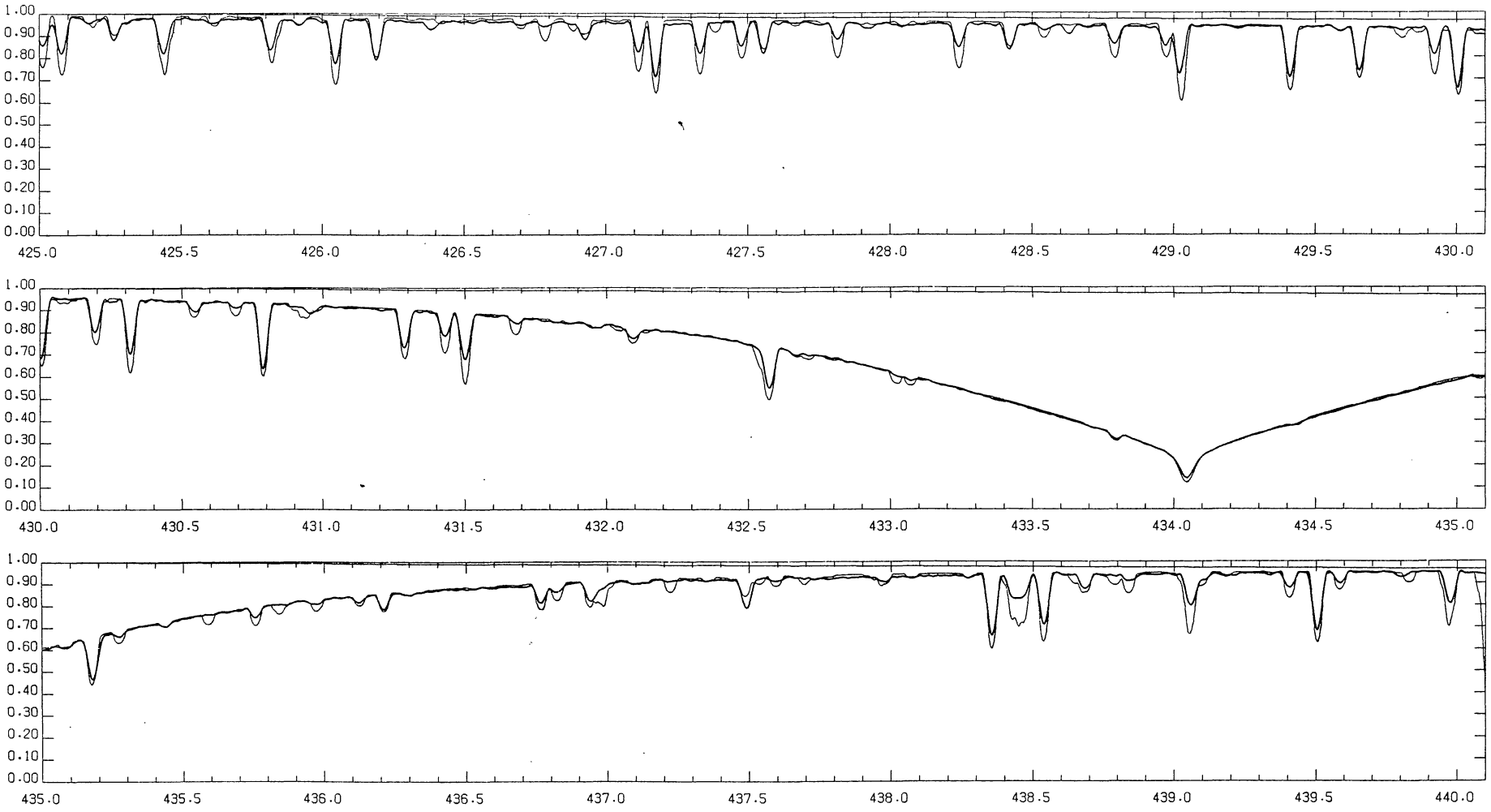

strong. Most of the features are made of iron group lines so that the assumption of 10 times overabundance in the iron group is too large by a factor of 2 or 3. We could obtain much better agreement simply by lowering the iron abundance and recomputing the spectrum. At least in the visible, a model with abundances scaled 10 times solar overestimates the opacity and should not provide a realistic temperature discribution. However, the line data in the ultraviolet are much less complete, and on Copernicus spectra a significant fraction of the lines is missing, so that an overestimate of the abundances may compensate in a model for the missing lines. Because of the large errors in the abundances it is difficult to draw any conclusions about the reliability of the gf values. Feature by feature comparisons will be made in the future to pick out obvious discrepancies.

Going through Kohl's (1964a) list for lines that are present in our atlas we note the following (ignoring errors in gf values and microturbulent velocity): Mg II at 439.1 nm, Al I at 396.2 and 394.4 nm, and S II at 416.3 nm are computed too strong, which probably indicates that we have overestimated the abundances by assuming 3 times solar. Mg I at 416.7 is calculated weak, probably indicating that the model is too hot. Sc II at 416.3 nm matches approximately so that an abundance of 1/10 solar is approximately correct. Sr II at 421.6 and Zr II at 355.2 are approximately correct with 10 times solar abundance. Y II lines at 363.3, 360.1, 361.1, and 362.9 are computed too weak at 10 times solar abundance.

There are lines of lighter elements present that arise from very high excitation levels but any interpretation is completely model dependent, so we will reserve discussion of those lines until we have a better model. Also many of the lines used in previous abundance analyses fall outside our short-wavelength interval. Light elements are present as resonance lines in our Copernicus spectrum that we analyze in the second paper in this series.

Not one single line of He is apparent in our observed spectrum although He lines are present in the predicted spectrum, 402.6 nm, for example. Either the model is too hot and is overpopulating the levels in the calculation, or helium is underabundant, or both.

The hydrogen line profiles are not reliable because they essentially have been fitted to the model calculation by adjusting the observed spectrum to match approximately the calculated spectrum. We can still discuss the shape of the line cores and the confluence of the Balmer series. The observed cores are always shallower, but that may simply represent the effect of scattered light, which has not yet been removed. However the shapes appear to be significantly different in that the dip of the core is more pronounced in the calculation than in the observation. This may be the result of some minor shortcoming of the Balmer line opacity routine. The effect must be model dependent because of the large temperature drops at the surface of enhanced abundance models so it may be greatly reduced once the spectrum is firmly calibrated and the calculation is redone with a better model. The Balmer line confluence is less contrasty in the observed spectrum than in the calculated, which indicates that we are underestimating the broadening. This is not surprising since the broadening theory is valid only for isolated lines. The last discernible line seems to be H_{19} at 368.6 nm in both spectra. The discrepancy in slope between 365 and 368 nm may be exaggerated because of the rapid change in exposure in the ultraviolet. We also underestimate the opacity in our treatment of merging lines below 366.4 nm (note the little steps in Figure 8) but there is no question that the treatment converges on the limit.

We can draw a number of interesting conclusions from the Ca II K line at 393.4 nm. First the unsmoothed profile in Figure 3 shows no sign of a circumstellar or interstellar component superimposed on the stellar profile. This is consistent with an estimate by John Black (1979) that the interstellar feature would appear at +18 km/sec with an equivalent width of 0.25 mA based on an extrapolation from the Mg II line observed by Kondo et al. (1978). Our signal to noise is not high enough to show such a feature. It would be worthwhile to get a very high signal to noise profile of the K line to search for it.

The smoothed Ca profile in Figure 3 is also symmetric and agrees qualitatively with the profile published by Griffin and Griffin (1979). There is no sign of the asymmetry found by Freire et al. (1977).

Turning to the smoothed stellar K line profile in Figure 8, we see that the observed line is even weaker than our prediction with 1/10 solar abundance. Thus Ca has the classical metallic line Ca underabundance contrary to earlier abundance analyses by Kohl (1964a); Strom, Gingerich, and Strom (1966); Latham (1969), and

Gehlich (1969).* If we look at the 422.7 line of Ca I however, we find that the calculated line is much weaker than the observed feature. A possible explanation for this is that as Ca I is a very minor state of ionization in Sirius it is strongly model dependent and difficult to interpret. The choice of a cooler model, as discussed earlier, would strengthen the Ca I lines.

In future work we plan to compute models for Sirius with self-consistent abundances and lower effective temperatures so that we may, it is hoped, settle on a "final" model.

*In a 1979 preprint, R.J. Panek and D.R. Stutman discuss the Ca H and K lines in Sirius and find a strong underabundance.

1979SAOSR.387.....K

5. REFERENCES

ALLER, L.H.

1963. The Atmosphere of the Sun and Stars. 2nd ed., The Ronald Press Co., New York, 650 pp.

BLACK, J.H.

1979. Personal communication.

BUSER, R., and KURUCZ, R.L.

1978. Theoretical UBV colors and the temperature scale for early-type stars. Astron. Astrophys., vol. 70, pp. 555-563.

CODE, A.D.

1975. Empirical effective temperature, bolometric corrections, and fundamental stellar properties. In Multicolor Photometry and the Theoretical H-R Diagram, ed. A.G.D. Philip and D.S. Hayes, Dudley Obs. Rep. No. 9, pp. 221-240.

CODE, A.D., DAVIS, J., BLESS, R.C., and HANBURY BROWN, R.

1976. Empirical effective temperatures and bolometric corrections for early-type stars. Astrophys. Journ., vol. 203, pp. 417-434.

CODE, A.D., and MEADE, M.R.

1976. Ultraviolet photometry from the Orbiting Astronomical Observatory. An atlas of ultraviolet stellar spectra, Wisconsin Astrophysics No. 30.

DAVIS, J.

1974. Unpublished.

DAVIS, J., and WEBB, R.J.

1974. Visual spectrophotometry of early-type stars. Mon. Not. Roy. Astron. Soc., vol. 168, pp. 163-175.

FREIRE, R., CZARNY, J., FELENBOK, P., and PRADERIE, F.

1977. High resolution profiles in A-type stars: I. The Ca II K line observed with the Meudon solar tower. Astron. Astrophys., vol. 61, pp. 785-796.

FURENLID, I.

1973. A method for calibration of stellar spectra. Amer. Astron. Soc. Photo-Bull., no. 1, pp. 15-17.

FURENLID, I.

1978. Signal-to-noise of photographic emulsions. In Modern Techniques in Astronomical Photography, ed. by R.M. West and J.L. Heudier, E.S.O., Geneva.

GEHLICH, U.K.

1969. Differential fine analysis Sirius versus Vega. Astron. Astrophys., vol. 3, pp. 169-178.

GRAY, D.F.

1973. On the existence of classical microturbulence. Astrophys. Journ., vol. 184, pp. 461-471.

GRIFFIN, R., and GRIFFIN, R.

1979. High resolution profiles in A-type stars. I. The Ca II K line in Sirius. Astron. Astrophys., vol. 71, pp. 36-37.

HAYES, D.S.

1967. Unpublished.

1979. Personal communication.

HAYES, D.S., and LATHAM, D.W.

1972. Unpublished.

1975. A rediscussion of the atmospheric extinction and the absolute spectral energy distribution of Vega. Astrophys. Journ., vol. 197, pp. 593-601.

JAMAR, C., MACAU-HERCOT, D., MONFILS, A., THOMPSON, G.I., HOUZIAUX, L., and WILSON, R.

1976. Ultraviolet bright star spectrophotometric catalogue. ESA SR-27.

JOHNSON, H.L., and MITCHELL, R.I.

1975. Thirteen-color photometry of 1380 bright stars. Revista Mexicana de Astron., vol. 1, p. 299.

KOHL, K.

1964a. Die atmosphäre des Sirius. Zs. f. Astrophys., vol. 60, pp. 115-164.

1964b. Das spektrum des Sirius von 3100-8863 A. Sonderdruck Sternwarte, Kiel.

KONDO, Y., TALENT, D.L., BARKE, E.S., DUFOUR, R.J., and MODISETTE, J.L.

1978. On the column density of the interstellar Mg II to Sirius and other nearby stars. Astrophys. Journ. (Lett.), vol. 220, pp. L97-L102.

KURUCZ, R.L.

1970. ATLAS: A computer program for computing model stellar atmospheres. Smithsonian Astrophys. Obs. Spec. Rep. No. 309, 291 pp.

1979a. Model atmospheres for G, F, A, B, and O stars. Astrophys. Journ. Suppl., vol. 40, pp. 1-340.

1979b. Problems of Calibration of Multicolor Photometric Systems. Dudley Obs. Report No. 14, ed. by A.G.D. Philip, pp. 271-296.

KURUCZ, R.L., and PEYTREMANN, E.

1975. A table of semiempirical gf values. Smithsonian Astrophys. Obs. Spec. Rep. No. 362 (in 3 parts), 1219 pp.

KURUCZ, R.L., TRAUB, W.A., CARLETON, N.P., and LESTER, J.

1977. The rotational velocity and Ba abundance of Sirius. Astrophys. Journ., vol. 217, pp. 771-774.

LATHAM, D.W.

1969. Abundances of the elements in Sirius and Merak. Smithsonian Astrophys. Obs. Spec. Rep. No. 321.

1974. Detective performance of photographic plates. In Methods of Experimental Physics, ed. by N.P. Carleton, Academic Press, Inc., New York, vol. 12.

MICHAUD, G.

1977. Stratification of elements in a quiet atmosphere: Diffusion processes. In IAU Highlights of Astronomy, ed. by E.A. Müller, vol. 4, part II, pp. 177-191.

PETERSON, D.M.

1968. The Balmer lines in early-type stars. Smithsonian Astrophys. Obs. Spec. Rep. No. 293, 199 pp.

1979. Personal communication.

PEYTREMANN, E.

1972. Theoretical effect of various broadening parameters on ultraviolet line profiles. Astron. Astrophys., vol. 17, pp. 76-82.

RELYEA, L.J., and KURUCZ, R.L.

1978. A theoretical analysis of uvby photometry. Astrophys. Journ. Suppl., vol. 37, pp. 45-69.

SAHAL-BRECHOT, S., and SEGRÉ, E.

1971. Semi-classical calculations of electron and ion collisional broadening of the strongest U.V. ionic lines of astrophysical interest. Astron. Astrophys., vol. 13, pp. 161-168.

SCHILD, R., PETERSON, D.M., and OKE, J.B.

1971. Effective temperatures of B- and A-type stars. Astrophys. Journ., vol. 166, pp. 95-108.

SMITH, M.A.

1976. Applications of Fourier analysis to broadening of stellar line profiles. II. A saturated line in 32 Aquarii and in Sirius. Astrophys. Journ., vol. 203, pp. 603-609.

STROM, S.E., GINGERICH, O., and STROM, K.

1966. Studies in non-gray stellar atmospheres. III. The metal abundances of Sirius and Vega. Astrophys. Journ., vol. 146, pp. 880-913.

TÜG, H,, WHITE, N.M., and LOCKWOOD, G.W.

1977. Absolute energy distributions of α Lyrae and 109 Virginis from 3295 Å to 9040 Å. Astron. Astrophys., vol. 61, pp. 679-684.

VAUCLAIR, G.

1976. On the problem of calibration between Am and δ-Scuti or "normal" A stars. Astron. Astrophys., vol. 50, pp. 434-444.

VIDAL, C.R., COOPER, J., and SMITH, E.W.

1973. Hydrogen Stark broadening tables. Astrophys. Journ. Suppl., vol. 25, pp. 37-136.

Figure 8. The calculated continuum, calculated unbroadened and 16 km/sec rotationally broadened spectra, the observed spectrum (heavy line), and line identifications plotted in 0.8-nm panels. No attempt has been made in the calculation to force a match to the observed spectrum. The observed spectrum has been roughly scaled to the calculated spectrum. The observed hydrogen line profiles are not reliable in this scaling. The dips in the calculated rotationally broadened spectrum at 360, 380, 400, 420, and 440 nm are artifacts of the broadening procedure that occur at edges of wavelength intervals. The line identifications consist of the last three digits of the wavelength, the element and ion code, the lower energy level in cm^{-1}, and the residual flux in per mil at line center if the line were computed in isolation. For example, in the first panel

232 24.01 38315 993 means
232 wavelength 352.8232 nm ,
24 atomic number Cr ,
.01 charge Cr^{+} = Cr II ,
38315 lower energy level in cm^{-1} ,
993 0.993 residual flux .

Full scale H_λ at the surface of Sirius is listed in the upper-left corner in units of $ergs/cm^2/sec/ster/nm$.

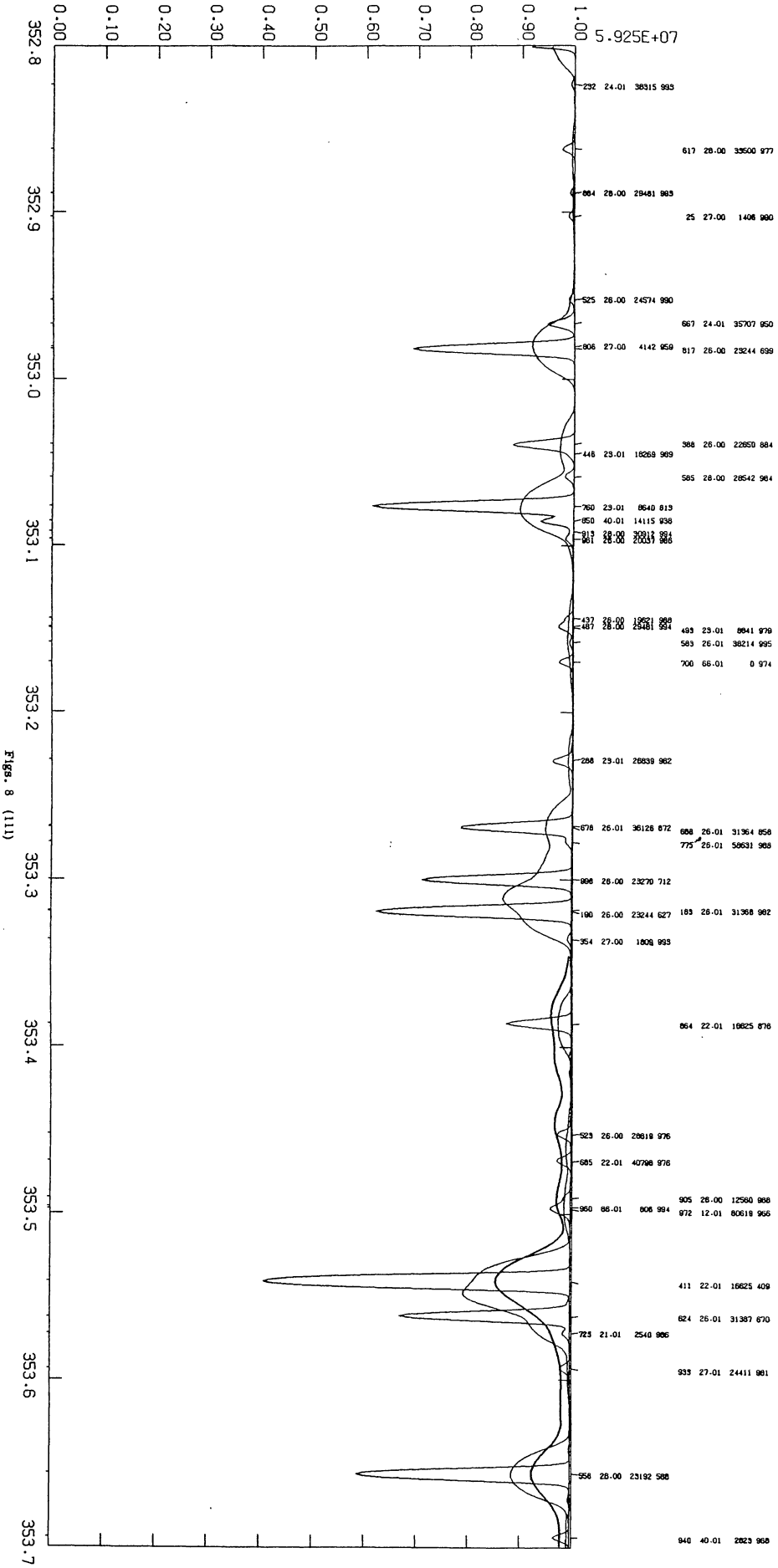

Figs. 8 (111)